Transient Eddy Forcing of Low-Frequency Atmospheric Variability

WERNER METZ

Meteorological Institute, University of München, Federal Republic of Germany

(Manuscript received 19 August 1986, in final form 16 February 1987)

ABSTRACT

This paper is concerned with the forcing of the low-frequency variability (10 days up to 3 months) of the barotropic planetary waves (wavenumbers 1 to 4) for wintertime conditions in the Northern Hemisphere. In particular, the forcing by the transient vorticity fluxes arising from the interactions between the planetary waves and the synoptic-scale eddies is considered. This forcing effect is stochastically modeled in terms of a combined Markov–complex EOF approach. The performance of these stochastically modeled vorticity fluxes is evaluated in the framework of a simple barotropic dynamical model.

It turns out that the forcing is highly coherent in wavenumber space, i.e., local in physical space, and that this organization is largely associated with its low-frequency components. The simple dynamical model with the modeled forcing is able to reproduce reasonably well the spatial structure of the observed low-frequency variance of the planetary waves. The performance is best if only the low-frequency components of the stochastically modeled forcing are prescribed. In this case the observed variance maximum over the Atlantic is well simulated, in position and in intensity, while the model variance over the Pacific is weaker than observed and shifted to the west.

1. Introduction

Blackmon (1976) defines the low-frequency regime of atmospheric flow as oscillations having periods greater than 10 days. Analyses of the 500 mb height field by Blackmon and White (1982) and Wallace and Blackmon (1983) suggest that a low-frequency filtering virtually acts as an implicit space filtering in the sense that the ultralong waves (wavenumbers $m \leq 4$) account for by far the largest part of the observed low-frequency (and also total) variance of the 500 mb height, while the high-frequency eddies (periods between 3 and 6 days, say) are represented mainly by shorter waves (synoptic-scale eddies).

Gall et al. (1979) proposed a mechanism to explain the low-frequency variability of the atmosphere. In particular, they considered the forcing of the low-frequency planetary waves by high-frequency synoptic-scale eddies. They used a simplified general circulation model with a baroclinically unstable zonal mean initial state. They found that besides the conversion from available potential energy, the ultralong waves received energy also by nonlinear transfer from the baroclinically growing synoptic-scale eddies. From a similar experiment Young and Villere (1985) concluded correspondingly that both processes are important for the growth of the planetary waves. Moreover, they stated that the direct transfer of kinetic energy from the intermediate-scale waves to the long waves can be inhibited by the heat transport.

These findings agree with the hypotheses of Wallace and Blackmon (1983) and Hoskins (1983) that the effect of the high-frequency eddies is to force the low-frequency waves via vorticity fluxes, while they act as a damping mechanism via the heat fluxes. This view gets additional support from Egger and Schilling (1983) who succeeded in explaining a large amount of the observed low-frequency variance just by forcing a barotropic planetary wave model with the observed transient synoptic-scale vorticity fluxes. Furthermore, using a similar model, Metz (1986) showed that the synoptic-scale transient eddy vorticity forcing contributes significantly to the maintenance of observed Northern Hemisphere blockings.

The starting point for the present study is the theory of Egger and Schilling (1984, referred to as ES in the following). These authors demonstrated most impressively that the autocovariances of observed planetary wave modes may be largely recovered by assuming that the temporal behavior of the planetary waves is governed by the theory of a stochastically driven, dissipative flow. Their forcing mechanism is due to the vorticity fluxes arising from the interaction between the planetary and the synoptic wave regimes, and the whole theory makes the equivalent barotropic assumption. They approximated the temporal behavior of the individual forcing modes in terms of a coupled Markov process for the sine and cosine wave components respectively.

In the present paper, we extend the approach of ES by representing the forcing in terms of a stochastic model which takes account of the observed correlations between the individual spectral forcing modes. This model is based upon a complex empirical orthogonal

function (EOF) analysis of the observed forcing time series whereby the temporal behavior of the EOF amplitudes is modeled in terms of complex Markov processes. We then use the simple dynamical model of ES with the Markov–EOF modeled to forcing to evaluate the spatial structure of the forced variance of the planetary-scale waves.

The paper is organized as follows. The data that are used for the evaluation of the forcing are described in section 2. Section 3 gives the theoretical background; in particular, we discuss the low-order dynamical model and the concept for the stochastic modeling of the forcing mechanism. In section 4 the skill of the forcing effect is evaluated by diagnosing observed data. Section 5 presents details of the complex EOF analysis and the fitting of the Markov models. The results of the integrations of the low-order dynamical model with the stochastic forcing included are presented in section 6 and the results are discussed and conclusions are drawn in section 7.

2. Data

The dataset used in this study is six winters (1979/80 to 84/85, each 110 days starting from 20 November) of daily 0000 UTC analyses from the European Centre for Medium Range Weather Forecasts. From these analyses we used the fields of the horizontal wind or the vorticity which were available in the form of global spherical harmonics coefficients (triangular truncation T45). Standard formulae were applied to obtain longitudinal Fourier coefficients of the streamfunction at Gaussian latitudes, and from these, hemispheric (odd) streamfunction spherical harmonic coefficients were obtained. Only a subtruncation (T16) of coefficients was retained.

Thus, at each standard level the streamfunction ψ is explicitly given by

$$\psi(\lambda,\varphi,t)=\sum_{m=-16}^{16}\sum_{n=|m|+1}^{6}\psi_n^m(t)P_n^m(\sin\varphi)\exp(im\lambda), \quad (1)$$

where the second sum is taken in steps of 2 and $\psi_n^{-m}=\psi_n^{*m}$. By virtue of (1) the streamfunction is represented by 72 complex coefficients. Time series of these coefficients were evaluated at standard levels 850, 700, 500, 300 and 200 mb. Using this data we computed at each level the spectral components of the synoptic-scale vorticity forcing (for definition see section 3), where the method of spectral interaction coefficients was used to evaluate the nonlinear Jacobians. The forcing actually used in the present study was obtained by vertical averaging of the spectral forcing modes. The same vertical averaging was applied to arrive at the time series for the planetary barotropic flow modes (for definition see section 3).

3. Theoretical approach

As mentioned before, the theoretical framework for the present study is provided by the work of ES. We shall follow the dynamical concept of ES, but with a different representation of the forcing.

a. Dynamical low-order model

The dynamical low-order model for barotropic planetary waves used in this study is essentially that described by ES. It is briefly summarized in the following.

The barotropic streamfunction ψ is decomposed into a planetary-scale part ψ_I and a synoptic-scale part ψ_{II} ($\psi=\psi_I+\psi_{II}$). This decomposition (see below) is performed in terms of spherical harmonic components. Inserting it into the equivalent barotropic vorticity equation and retaining only the projection onto the planetary-scale modes yields

$$\partial/\partial t(\nabla^2-\Lambda^{-2})\psi_I=-\{2\Omega/a^2+U_0/a(2/a^2-\nabla^2)\}\times\partial\psi_I/\partial\lambda-k\nabla^2\psi_I+A\nabla^4\psi_I+F(t), \quad (2a)$$

where

$$F(t)=-J_I(\psi_{II},\nabla^2\psi_I)-J_I(\psi_I,\nabla^2\psi_{II})-J_I(\psi_{II},\nabla^2\psi_{II}). \quad (2b)$$

The dynamical model (2a) is linear as it neglects the nonlinear Jacobian arising from the interaction between the planetary waves themselves. Furthermore the superrotational part of the streamfunction is considered separately, i.e., $\psi_I=-aU_0\sin\varphi+\psi_I'$; the primes have been dropped in (2a). All the symbols in (2a, b) have their usual meanings; A and k are coefficients of Ekman friction and diffusion, Λ is a Rossby radius of deformation, $F(t)$ is the vorticity forcing, which comprises the effects of both synoptic–synoptic as well as synoptic–planetary wave interactions on the planetary waves. As will be described in the second part of this section, we represent $F(t)$ in terms of a stochastic model.

The parameters occurring in (2a) are prescribed according to $U_0=10.7$ m s^{-1} (i.e., the climatological winter mean), $\Lambda=1000$ km, $k=1/(15$ days) and $A=0.8\times10^6$ m^2 s^{-1}. In this study the definition of the planetary-scale waves is different from ES. In particular, we consider as planetary waves all the spectral modes that are obtained from a rhomboidal truncation with $|m|\leq 4$ and $n-|m|\leq 7$, i.e., altogether 20 complex coefficients. The complement with respect to the basic truncation (T16) is called the synoptic-scale wave regime.

b. Representation of F(t)

Although ES did not mention it explicitly, their stochastic model for the temporal behavior of the forcing

modes $F_n^m(t)$ may be conveniently written in terms of a complex Markov process:

$$F_k = \alpha F_{k-1} + w_k, \tag{3}$$

where k is discrete time and the wavenumber indices (m, n) have been dropped. The w_k is a complex white noise process. The Markov process (3) has a complex autocorrelation function

$$R(\tau) = \exp(-b|\tau| - i\omega\tau), \tag{4a}$$

with

$$b = -\ln|\alpha| \quad \text{and} \quad \omega = -\arg(\alpha). \tag{4b}$$

Least-squares estimates of α and $\sigma^2(w)$ may be obtained from

$$\alpha = \langle F_k F_{k-1}^* \rangle / \langle F_k F_k^* \rangle, \tag{5a}$$

$$\sigma^2(w) = (1 - \alpha\alpha^*)\langle F_k F_k^* \rangle, \tag{5b}$$

where the angle brackets denote a time averaging. Note that by virtue of (5a), ω is just the linear phase speed of the wave modes, while b^{-1} is their persistence.

Our modification of ES's approach (3) is to consider possible correlations among the forcing modes. The most convenient way to solve this problem is to make use of a complex empirical orthogonal function analysis of the observed forcing, i.e., to evaluate the eigenvectors of the Hermitian covariance matrix of the spectral forcing modes

$$H_{ij} = \langle F_i F_j^* \rangle, \tag{6}$$

where now i and j are shorthand notations for the I wavenumber vectors (m_i, n_i) and (m_j, n_j). The forcing may then be expanded in terms of the eigenvectors V_i^l obtained from such an analysis (l indicates that the eigenvector is associated with the lth eigenvalue p_l)

$$F_{k,l} = \sum_{l=1}^{L} Q_k^l V_i^l, \tag{7}$$

where k is again time and L is the total number of eigenvalues resulting from the analysis. The Q_k^l are the time-dependent complex amplitudes of the expansion and they do not depend on wavenumber index i. These amplitudes may be obtained by projecting the observed forcing onto the eigenvectors

$$Q_k^l = \sum_{i=1}^{I} F_{k,i} V_i^{*l}. \tag{8}$$

The important point is now that, because the eigenvectors V_i^l are orthogonal in space, the amplitudes Q_k^l are orthogonal in time, i.e.,

$$\langle Q_k^l Q_k^{*l'} \rangle = \delta_{ll'} p_l. \tag{9}$$

Therefore, the behavior of the Q may be readily modeled by independent complex Markov processes parallel to (3):

$$Q_k^l = \alpha^l Q_{k-1}^l + w_k^l. \tag{10}$$

Here l denotes the lth eigenvalue and k time. Insertion of (10) into (7) yields the stochastic model for the forcing modes that is used in this study:

$$F_{k,i} = \sum_{l=1}^{L'} (\alpha^l Q_{k-1}^l + w_k^l) V_i^l. \tag{11}$$

By writing L' instead of L we indicate that normally the sum in (11) is restricted to a subset of eigenvectors; in particular, we shall retain only those eigenvalues which turn out to be statistically significant (see section 5). The information about the correlations and among the forcing modes is contained in the eigenvectors. Details of the complex EOF analysis and the fit of the Markov models (10) are described in section 5.

The dynamical model (2a) is solved with the forcing represented by (11). As each forcing mode is composed by a sum of terms, an analytical solution of (2a) as in ES is no longer possible. Instead, we solve the model by means of numerical integration, details which are given in section 6.

4. Skill of $F(t)$

Before turning to the stochastic modeling let us first examine the skill of the observed forcing to explain the observed tendencies of the planetary waves. For that purpose, we have evaluated in wavenumber space the complex correlations

$$C(d\psi/dt, F) = \langle d\psi/dt F^* \rangle / (\langle d\psi/dt d\psi^*/dt \rangle \langle FF^* \rangle)^{1/2} \tag{12}$$

between the corresponding spectral modes (again wavenumber indices are omitted). The time mean and a quadratic least-squares fit to the seasonal trend were removed from the time series. Low-frequency components were obtained by applying a low-pass filter which retains only oscillations having periods of more than 10 days (Blackmon and Lau, 1980). The tendencies were calculated by means of a centered-difference operator with $\Delta t = 1$ day.

As usual, we define the (temporal) skill in terms of the squared modulus of the complex correlation (CC^*). Furthermore, the argument of C represents the phase shift in longitudinal direction between the two waves, at which maximal skill is found. A 95% significance threshold for the Cs is evaluated as twice the standard deviation of correlations which occur between random red noise data that have the same persistence characteristics [cf. (4a, b)] as the actual data (see Metz, 1986). In the following, only statistically significant correlations were displayed as vectors in the complex plane with the real axis to the right and the imaginary axis upwards.

The complex correlation vectors C and isolines of the skill CC^* are shown for the unfiltered data in Fig.

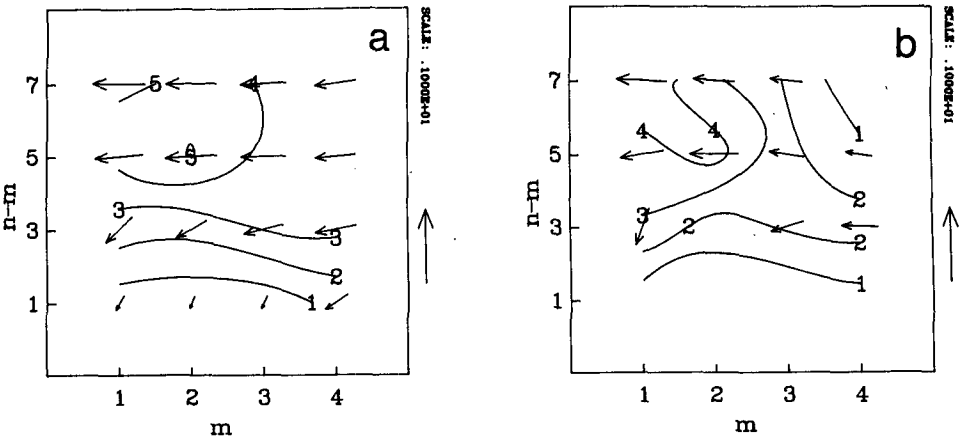

FIG. 1. Complex correlation $C(d\psi/dt, F^*)$ at zero lag. Correlations are represented by vectors in complex plane with real axis to the right and imaginary axis upwards. Contour intervals of skill (CC^*) in units of 0.1 (a) for observed unfiltered data and (b) for observed low-pass filtered data. Statistically insignificant (see text) correlations are omitted.

1a and for the low-pass filtered data in Fig. 1b. At first glance, both figures look rather similar which suggests that the major contribution to the skill of the forcing effect is associated with the low-frequency components. Virtually an $-\pi$ out of phase relationship [recall that by virtue of (2a) the streamfunction tendencies and the forcing are negatively correlated] can be observed at high meridional modes $n - |m| = 5.7$ for both the analysis of the unfiltered as well of the low-pass filtered data. In this region of wavenumber space we find skill values of up to 50% (Fig. 1a) and 40% (Fig. 1b). The skill for the low-pass filtered data becomes smaller at zonal wavenumber $m = 3$ and, particularly, $m = 4$. The tilting of the vectors at $n - |m| = 3$ indicates together with a reduced skill that the forcing is less effective for these modes. The situation is extreme at modes with $n - |m| = 1$ where this forcing effect has virtually no skill, i.e., the correlations are not significant for the low-pass filtered data.

Our analysis compares well with the results of ES if the structure of the skill values in wavenumber space is considered. However, our skill values are twice as large as the values presented by ES. This difference may be due to the facts that ES used a different dataset, that they considered data for the whole calendar year, and that they used a slightly different definition for the planetary waves. Kruse and Hasselmann (1986) and Barnett and Roads (1986) have diagnosed the skill of the total Jacobians in the 500 mb barotropic vorticity equation. Both studies find a skill of about 10–20% which agrees with the results of ES. Furthermore, as both studies use the same data as ES one may conclude that the nonlinear interactions between the planetary-scale waves themselves (which have been omitted by ES) do not tend to increase, but rather to mask the skill due to the synoptic-scale forcing. A similar analysis by Bruns (1985) has been performed on the basis of a two-level model. Bruns has also examined the effect of the synoptic-scale forcing and found skill values of about 10%. However, his results are virtually noncomparable with ours, as he used a rather extreme definition of the planetary waves by including wavenumbers up to $m = 8$.

In summary we state that the synoptic-scale forcing has a high skill in explaining the observed variance of the tendencies of the planetary barotropic flow. This effect is mainly due to the low-frequency components and concentrated at modes with $n - |m| = 5.7$ and $m = 1$ to 3. The modes with a large meridional scale $n - |m| = 1$, however, are exceptional in that they are virtually not forced by this mechanism.

5. Stochastic modeling of $F(t)$

In this section we first present the results of the EOF analysis of the forcing and then the fit of the Markov models to the EOF amplitudes.

a. EOF analysis

A complex EOF analysis of the forcing has been performed by following the technique described, e.g., in Barnett and Roads (1986). In particular, we computed the Hermitian covariance matrix (6) for the forcing using the detrended time series of the complex spectral components of $F(t)$. As $F(t)$ has no component that contributes to the change of the superrotational flow ($m = 0$, $n = 1$) 19 real eigenvalues and complex eigenvectors are the outcome of this analysis.

The eigenvalues obtained from the EOF analysis of the unfiltered data are shown in Fig. 2. They are ordered by magnitude and scaled to represent just their partial contribution to the total variance. The first eigenvalue

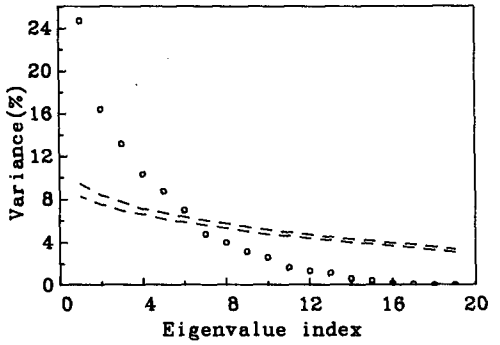

FIG. 2. Eigenvalues obtained from complex EOF analysis of unfiltered forcing modes (open circles). Dashed curves represent (5%–90%) probability interval for eigenvalues obtained from random data. (See text for further explanation.)

is well separated (330 degrees of freedom) from the others and captures 24.7% of variance. Additionally shown in Fig. 2 is a 5%–95% probability interval for eigenvalue curves that can occur for random data. This interval has been evaluated by a Monte Carlo technique in parallel to Preisendorfer et al. (1981). However, it has been assumed that the random data are red noise uncorrelated in space, having the same persistence characteristics as the observed data. In particular, the red noise was obtained from a Markov model in parallel to (3), where α has been evaluated from the data but $\sigma^2(w) = 1$ for all modes. The test identifies the first six eigenvalues to represent statistically significant information. We have also examined the stationarity of the process by decomposing the total dataset into two parts and repeating the EOF analysis for the first and last three winters separately. The outcome of this computations was nearly identical; the most important eigenvalues represented 25.9% and 24.2% of variance, respectively.

The structure in wavenumber space of the leading eigenvector is shown in Fig. 3. Here, the contributions from the individual spectral modes to the eigenvector are displayed as vectors in the complex plane. As the phase of the eigenvector components is obtained only relative to an unknown constant, the components of the vector were arranged such that zero phase is assigned to the component with the largest absolute value. In Fig. 3 this largest component is associated with the smallest spatial scale (4, 11), the eigenvector having significant contributions only from wave modes with $m = 2, \cdots, 4$ and $n - |m| = 5.7$. It is interesting to observe that these significant elements of the eigenvector exhibit a highly coherent structure with respect to their relative phase differences. This means that the structure associated with this eigenvector in physical space is characterized by a clustered local pattern. We come back to this feature at the end of section 6. The structure of the remaining eigenvectors (not shown) becomes less and less ordered with increasing eigenvalue index.

As we have demonstrated above (section 4) the skill of the synoptic-scale forcing to explain the observed variability of the planetary-scale waves is mainly due to its low-frequency components. Therefore, we have also performed an EOF analysis of the low-pass filtered data. The eigenvalues obtained from this computation are shown in Fig. 4. The most striking difference from Fig. 2 is that, due to the increased persistence of the low-pass filtered data, the noise interval is much broader and closer to the curve of the computed eigenvalues. According to this test only the first four eigenvalues can be considered as statistically significant. A closer inspection reveals that the relative contribution of the leading eigenvalue has been decreased to 20.6% compared to the unfiltered case, while the relative contributions of the second to fourth eigenvalue remained virtually unchanged.

Figure 5 shows the structure in wavenumber space of the first eigenvector. The most important feature of this figure is that it is very similar to Fig. 3. This suggests that the spatially organized variability of the forcing is mainly due to its low-frequency components. One can

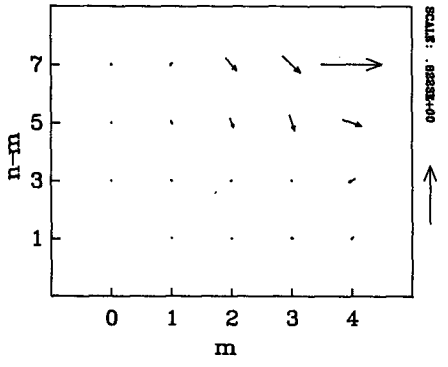

FIG. 3. Structure in wavenumber space of the eigenvector associated with the largest eigenvalue of Fig. 2 (24.7% of variance). Spectral components are represented as vectors in complex plane.

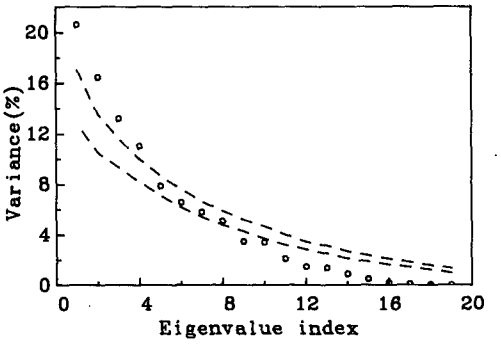

FIG. 4. As in Fig. 2 except for EOF analysis of low-pass filtered data.

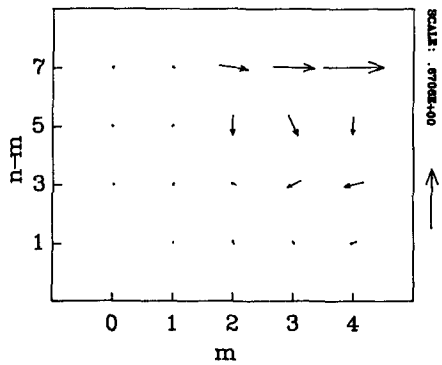

FIG. 5. Leading eigenvector as in Fig. 3 except for EOF analysis of low-pass filtered data.

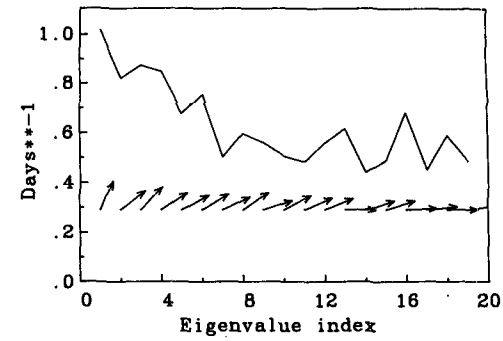

FIG. 6. Markov parameters b (full line) and ω (vectors) as obtained by fitting complex Markov processes to the observed EOF amplitudes of the unfiltered vorticity forcing. See text for further explanation.

also see that the largest wavemodes are even more coherent than that in Fig. 3, and that the relative influence of the smallest scale component (4, 11) has been reduced.

Our results exhibit a striking contrast to the EOF analysis of the total barotropic Jacobian presented by Barnett and Roads (1986), as these authors have found that the leading eigenvector did not exhibit any coherent structure. They concluded that the variability of the total Jacobian is associated with a virtually white structure in wavenumber space. This conclusion is obviously not valid for the synoptic-scale forcing.

b. *Stochastic model fit*

By projecting the time series of the observed, detrended forcing modes onto the eigenvectors [cf. (8)], we obtained time series of the observed EOF amplitudes. As discussed, e.g. by Horel (1984), these amplitudes described the temporal propagation in physical space of the EOF pattern. To model the temporal behavior of the amplitudes, we make use of the fact that, as outlined in section 3, the EOF amplitude time series are mutually uncorrelated.

Complex Markov models (10) were fitted to the EOF amplitude time series. Thereby, a least-squares strategy was used, i.e., the parameters α^l and $\sigma^2(w)^l$ were obtained in parallel to (5a, b) from the EOF amplitude time series. Figure 6 shows the parameters α^l for all 19 EOF amplitudes. Here, the full curve represents the parameter b [cf. (4b)] of the Markov process. Recalling that b^{-1} is just the persistence, Fig. 6 shows that the temporal variability associated with the EOF patterns is characterized by very low persistence. Typical values are about one day for the leading EOF increasing to about two days with increasing EOF index. These characteristics agree with the results of ES for the spectral forcing modes. Also shown in Fig. 6 is a series of vectors, the slope of which represents the parameter ω of the Markov process. For each spectral mode of an eigenvector ω gives just the linear phase speed of the associated wave. Furthermore, as the relative phase differences between the wave modes of an eigenvector are fixed, the whole EOF pattern also propagates with ω. It can be seen that all ω are positive, i.e., the associated EOF patterns are eastward moving. However, due to the low persistence which is characteristic of their time behavior, these moving pattern decay rather rapidly during about one or two days. The major part of the temporal variability of the individual EOF structures, however, is identified by the Markov model fit as white noise oscillations. This level of noise variance is as much as 80–90% for the leading statistically significant eigenvalues (Fig. 7).

It is a very convenient property of the complex EOF expansion that the spatial structure of the temporal variance (that is related to a particular eigenvector) is determined by the properties of the eigenvector alone, provided the time mean of the temporal phase is vanishing. This may easily be understood by considering the following simple example. A real physical quantity $X(\lambda, t)$ (for simplicity only λ dependent) may be given by time series of complex Fourier coefficients. Assume now that a complex EOF analysis of $X(\lambda, t)$ has been

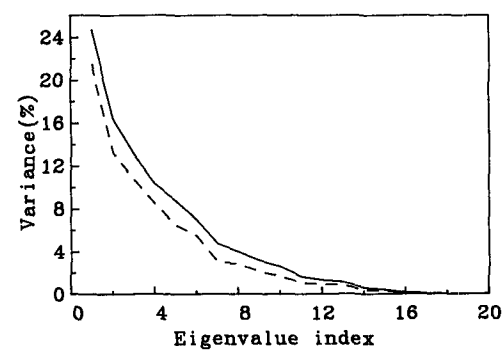

FIG. 7. Total (full) variances for forcing EOF amplitudes and residual (dashed) white noise variances as obtained by Markov fitting. See text for further explanation.

performed. An eigenvector resulting from this analysis shall, for simplicity, be composed just of two waves with zero (longitudinal) phase lag, e.g., in real notation $[\cos(\lambda) + \cos(2\lambda)]$. Then the contribution of this eigenvector to $X(\lambda, t)$ may be written as

$$Y(\lambda, t) = A(t) \cdot \{\cos[\lambda + \varphi(t)] + \cos[2\lambda + \varphi(t)]\}. \quad (13)$$

The real amplitude $A(t)$ and the phase $\varphi(t)$ may be obtained from the complex EOF amplitude as discussed above. The eigenvector pattern $Y(\lambda, t)$ may propagate in physical space by virtue of the time dependent phase $\varphi(t)$. The λ-dependence of the variance resulting from (13) is

$$\frac{1}{T}\int_0^T Y(\lambda, t)^2 dt = \frac{1}{T}\int_0^T A(t)^2 dt \cdot (1 + \cos\lambda), \quad (14)$$

where it has been assumed that the time integral may be replaced by an integral over 2π for the phase φ. The structure of the variance in physical space in (14) is independent of the phase $\varphi(t)$.

We have also fitted Markov models to the amplitude time series obtained from the complex EOF analysis of the low-pass filtered data. In this case (not shown) the rapidly fluctuating components of the forcing have been entirely filtered out and the EOF pattern in physical space is made up of very persistent, virtually in situ low-frequency oscillations.

For the numerical experiments to be described in the following section we used two stochastic models in parallel to (11) to represent the forcing. The first model (called high-frequency stochastic forcing) uses the first six eigenvectors and the parameters of the Markov process as obtained from the analysis of the unfiltered data, while the second model (called low-frequency stochastic forcing) was made up of the first four eigenvectors and Markov parameters for the low-pass filtered data.

6. Results

The response of the linear dynamical low-order model (2a) to the synoptic-scale forcing mechanism is evaluated by means of numerical integration. In particular, we describe here the outcome of three different experiments, where the first uses the forcing as observed, but detrended (run 1). The second (run 2) uses the high-frequency stochastic forcing model, as described before, while the third (run 3) uses the low-frequency stochastic forcing.

The dynamical model (2a) is integrated by means of a Runge–Kutta fourth-order scheme with a time step of 6 h. The forcing, as observed and as obtained from the two stochastic models respectively, is updated every fourth time step during the integrations and then kept fixed for the following three steps. Each run comprises six winter runs of 110 days each, whereby the first winter run is once repeated to establish statistical equilibrium. The initial conditions for each winter run were the state of the model flow at the last day of the preceeding winter run; the initial conditions for the first winter run were a purely superrotational flow. The Markov models for the stochastic forcing were started from zero and the white noise component was obtained from a normal distribution with zero mean and standard deviation $\sigma(w)$ (cf. section 5).

a. Temporal model skill

In parallel to section 4 we have evaluated the skill of the model flow with respect to the observed planetary flow. Obviously, this analysis can be made only for run 1, i.e., for the observed forcing. Figure 8 displays the complex correlations at lag zero between the low-frequency observed flow and the planetary flow predicted by model run 1. One recognizes nearly the same structure, except for a shift of π, as that obtained from the diagnostic analysis of the streamfunction tendencies and the forcing (Fig. 1b). However, the skill is generally lower for all wavenumbers. Actually, the skill shown here is the partial skill of the forcing mechanism in the presence of linear wave propagation and friction. This partial skill is still as high as more than 20% for the higher meridional modes of the zonal wavenumbers $m = 1, 2$.

b. Spatial skill

Let us now examine the structure in physical space of the streamfunction variance that is predicted by our model runs. The verification is against the variance of the observed low-frequency (i.e., low-pass filtered) planetary barotropic streamfunction. To evaluate the observed variance, seasonal trends were removed from the data, as described above. Thus the variance shown here is virtually due to oscillations having periods from 10 days up to 3 months. The local variances were eval-

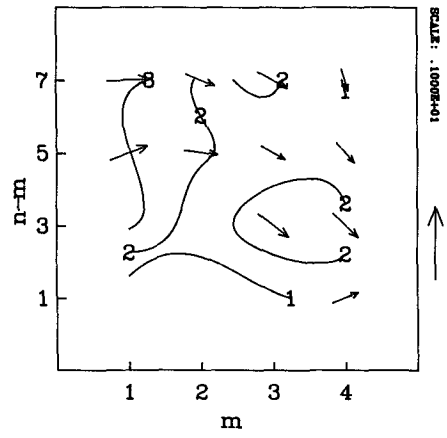

FIG. 8. Complex correlations and isolines of skill as in Fig. 1 except between low-pass filtered observed flow and model run 1 flow.

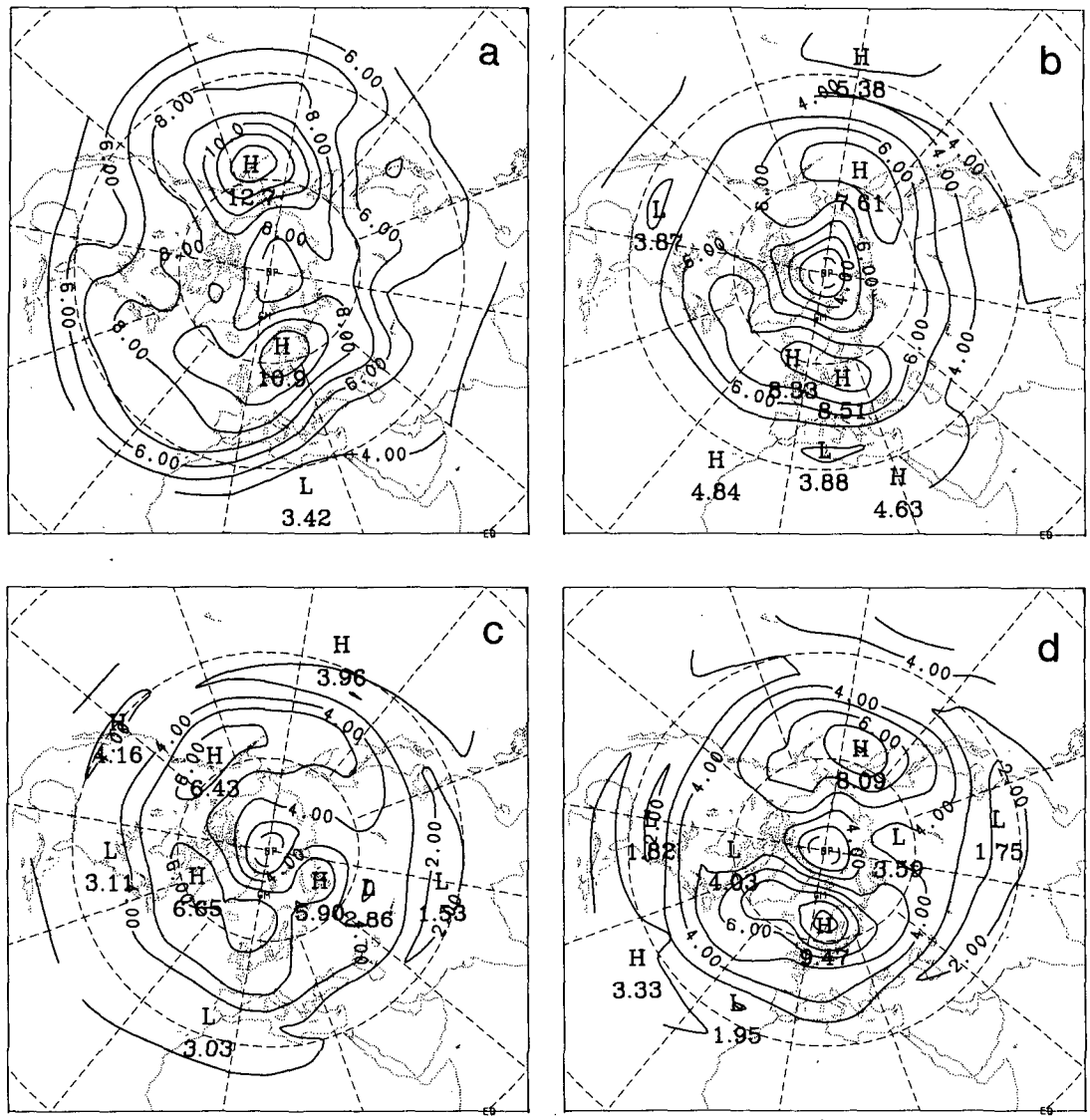

FIG. 9. Standard deviation of planetary barotropic streamfunction in 10^6 m^2 s^{-1}: (a) Observed wintertime low-pass filtered planetary waves, (b) model run 1 (observed forcing), (c) model run 2 (high-frequency stochastic forcing) and (d) model run 3 (low-frequency stochastic forcing).

uated from daily grid point values in a longitude–latitude grid with increments of 10 and 5 degrees, respectively. As usual, we do not display the variances themselves but the standard deviations instead.

Figures 9a–d show the standard deviations of the observed wintertime low-frequency planetary flow and of our model runs run 1, run 2 and run 3. As one can see all the models show skill in reproducing the observed maxima over Northern Europe and the Pacific Ocean, as well as regions of low variability over the American and Asian continents. A closer inspection reveals that model run 1 (Fig. 9b) does well in simulating the observed variability over Northern Europe; the Pacific maximum being shifted about 30 degrees to the west. The model (Fig. 9c) run 2 does less well, as it predicts the highest variability near 60°W and the Northern Europe and Pacific maxima are shifted eastward. Model run 3 (Fig. 9d), on the other hand, comes very close to the observed pattern over Northern Europe with respect to intensity and spatial structure. The Pacific response is somewhat weaker and shifted to the west.

All the models are successful in predicting the general increase of the variance from low to high latitudes and exhibit maximal variance around 60°N. The most interesting features of the spatial variance pattern, how-

ever, is its variation with longitude. To obtain a more objective measure of the performance of the individual models we have developed a parameter which measures the skill of the models in recovering the observed spatial structures. To compare spatial structures, a spatial scale for which the comparison should be performed must first be defined. On the basis of Fig. 9a we assume that the significant structures of the variance pattern may be recovered by using sectors of 60 degrees of longitude. As the most important information in Fig. 9a is concentrated near 60°N the meridional extent of the sectors was chosen as 75° to 50°N. Having thus defined the spatial scale for our analysis, we computed a skill parameter as follows.

The basis for the computations were the grid point values of the variance in a zonal belt from 75° to 50°N. The zonal mean was subtracted at each latitude circle. To compensate for spherical effects, the values along each latitude circle are weighted by the cosine of latitude. A 60-degree longitude wide test sector was then centered at a particular longitude. The linear trends with longitude and latitude in this test sector were removed from the grid point values. Finally, the skill parameter was defined as the spatial correlation between the test sectors of the observed variance and the model predicted variance. If the correlation happens to be negative, the skill parameter was set to zero. To take care of the stability of the skill parameter with respect to a longitudinal shift of the test sectors, the analysis was performed by shifting the test sector around the whole latitude belt in steps of 10 degrees longitude.

The outcome of this procedure is displayed in Fig. 10. The smooth full curve represents the observed variance along 60°N. The full curve indicates the longitudinal variation of the spatial skill of model run 1 in reproducing the observed variance pattern, the dashed curve refers to model run 2 and the open circles to model run 3. The experiment with the high-frequency stochastic forcing (run 2) exhibits virtually no skill in reproducing the observed local variance structure on the preselected scale. The experiment using the observed forcing (run 1) has high skill values at 90°E, i.e., just at those longitudes where the observed variance has a relative minimum. However, the model has also a high skill at the eastern margin of the observed Pacific maximum. The model with the low-frequency stochastic forcing (run 3), exhibits high skill values over a broad band of longitude ranging from 120°E to 170°W, which is related to the Pacific maximum. As opposed to the other models, this model is also able to capture the smaller-scale Northern Europe maximum at its correct position, as indicated by the high skill values from 10°W to 30°E. Note that this skill parameter is not sensitive to differences in amplitude. Thus, although run 3 comes closer in amplitude to the Atlantic maximum than to that over the Pacific, this is not reflected in the magnitude of the skill values. However, the spatial skill parameter is able to show up the other main features of the run 3 model response, namely, that the Pacific variance has a larger scale than the Northern Europe variance and, secondly, that the Pacific maximum is shifted about 30 degrees to the west with respect to the observed maximum, while that over Northern Europe is predicted at its correct position.

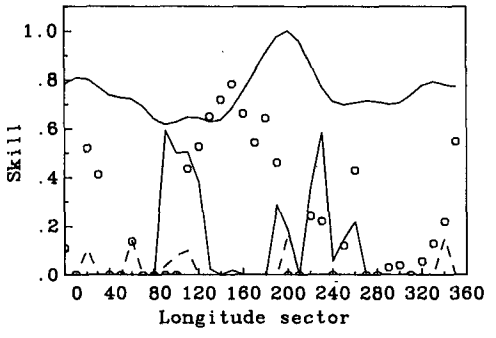

FIG. 10. Spatial skill parameter (see text). Model run 1 (full), model run 2 (dashed) and model run 3 (open circles). The smooth full curve is the observed variance at 60°N.

As a last point, we have evaluated the response of the model when only the leading eigenvector from the EOF analysis is used to generate the forcing where we have taken the eigenvector from the analysis of the low-pass filtered data. As we have already shown, this eigenvector exhibits a very coherent structure in wavenumber space (Fig. 5a); thus one can expect that the model response will be highly localized in physical space. Figure 11 displays the standard deviation resulting from this experiment. By comparison with Fig. 9d one can see that the leading EOF (20.6% of variance) virtually determines the structure of the run 3 response over Northern Europe. The (much weaker) secondary maximum found southward of the main response suggests that the variance pattern is at least partly due to a transient high–low dipole pattern commonly observed during European blocking. This finding helps to understand the results of Metz (1986) who showed that the average structure of Atlantic blocks may be recovered by using a similar model as in this study, but with observed forcing only.

7. Discussion and conclusions

We have examined the effect of the vorticity fluxes arising from the interaction between the transient planetary-scale and the synoptic-scale waves on the variability of the barotropic component of the planetary-scale waves themselves. Because, at zero lag, the planetary-scale waves are virtually independent of the vorticity fluxes and, furthermore, the vorticity fluxes provide an energy source term for the planetary waves,

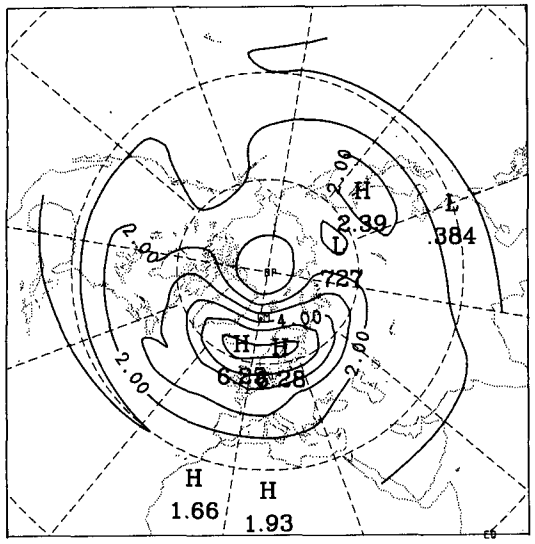

FIG. 11. As in Fig. 10 except for model run 3 with low-frequency stochastic forcing by the first eigenvector only.

these fluxes may be considered as a stochastic forcing mechanism of the planetary wave variability. This mechanism has been established by Egger and Schilling (1983).

The general picture of the nature of this mechanism that emerges from our results may be described as follows. As shown by ES, the temporal variability of the individual spectral forcing modes has the characteristics of a stochastic process. However, this is our first important result: a large fraction of the variability of the forcing is associated with highly coherent structures in wavenumber space, or equivalently with locally distinct regions in physical space. This finding may be easily understood if one recalls that the synoptic-scale eddies in the atmosphere occur primarily over distinct regions related to the stormtracks over the Atlantic and Pacific oceans. The second important outcome of this study is that this spatially organized structure of the forcing is associated primarily with its low-frequency components.

On the basis of these two findings we have demonstrated that the forcing mechanism may be modeled in terms of a combined Markov–complex EOF approach. The performance of this model for the forcing has been examined in the framework of a simple dynamical model for the planetary flow, virtually the same dynamical model as that used by ES. Our major result is that the simple dynamical model with the stochastically modeled forcing included is able to reproduce to a large extent the spatial structure of the observed low-frequency planetary wave variance. The model has the highest skill, if only the low-frequency components of the forcing are retained; the high-frequently oscillating parts of the forcing tend to obscure this effect. The structure and the intensity of the observed variance maximum over Northern Europe is well reproduced by the model. The Pacific maximum in the model has, correctly, a larger scale than that over Northern Europe; however, it is weaker and shifted about 30 degrees to the west. This suggests that our forcing mechanism has greater importance for the variability over the Atlantic than for that over the Pacific. This is also supported by the results of Metz (1986) who found that Atlantic blocks are better simulated by this effect than Pacific blocks. Additional support comes from a diagnostic study by Hansen and Chen (1982) who suggest that baroclinic processes may be of more importance for Pacific than for Atlantic blocks. Our findings concerning the low-frequency variance over the Atlantic are also in agreement with results of Hoskins et al. (1983) who evaluated the *E*-vectors from the high-pass filtered (retaining fluctuations up to seven days) transient eddies and compared its time mean contributions with the 12 day mean flow during an episode of Atlantic blocking. They found that the mean eddy fluxes as represented by the 12 day mean *E*-vectors tended to reinforce the block, whereby the 12 day mean *E*-vectors may be considered as representing the low-frequency components of the fluxes.

Finally, let us discuss the limitations of our model approach. We have neglected a number of important processes which may also contribute to the low-frequency variability of the planetary waves. These are, e.g., nonlinearity and barotropic stationary forcing (note that any stationary forcing effects have been omitted in this study), slowly changing external boundary conditions or, particularly, baroclinic interactions between the planetary waves. It remains to show how the model with the barotropic forcing mechanism works if one or more of these processes are included. Furthermore, it appears to be a major deficiency of our model that it does not take into account the feedback from the planetary into the synoptic scale. However, as is well known, this feedback occurs mainly via baroclinic processes and is closely related to baroclinic instability. This implies that a fully baroclinic model is required for that purpose. Since the feedback is an energy sink for the planetary waves, a straightforward extension of the model approach of this study to the baroclinic case appears not to be possible. Instead, a new model for the representation of the baroclinic fluxes must be developed.

Acknowledgments. The author is grateful to Prof. J. Egger, Prof. F. Schmidt, and D. Schilling for many helpful discussions. A. W. Robertson is thanked for carefully reading the manuscript. The NAG numerical library was used to solve the eigenvalue problem and the NCAR graphics package to prepare the sterographic projection maps. This work was supported by the German Federal Ministry of Research and Technology.

REFERENCES

Barnett, T. P., and J. O. Roads, 1986: Stochastic forcing and prediction of low-frequency planetary scale flow. *J. Atmos. Sci.*, **43**, 940–947.

Blackmon, M. L., 1976: A climatological spectral study of the 500 mb geopotential height of the Northern Hemisphere. *J. Atmos. Sci.*, **33**, 1607–1623.

——, and N.-C. Lau, 1980: Regional characteristics of the Northern Hemisphere wintertime circulation: A comparison of the simulation of a GFDL general circulation model with observations. *J. Atmos. Sci.*, **37**, 497–514.

——, and G. White, 1982: Zonal wavenumber characteristics of Northern Hemisphere transient eddies. *J. Atmos. Sci.*, **39**, 1985–1998.

Bruns, T., 1985: On the contribution of linear and nonlinear processes to the long-term variability of large-scale atmospheric flows. *J. Atmos. Sci.*, **42**, 2506–2522.

Egger, J., and H. D. Schilling, 1983: On the theory of the long-term variability of the atmosphere. *J. Atmos. Sci.*, **40**, 1073–1085.

——, and ——, 1984: Stochastic forcing of planetary scale flow. *J. Atmos. Sci.*, **41**, 779–788.

Gall, R., R. Blakeslee and R. C. Somerville, 1979: Cyclone-scale forcing of ultralong waves. *J. Atmos. Sci.*, **36**, 1692–1698.

Hansen, A. R., and T.-C. Chen, 1982: A spectral energetics analysis of atmospheric blocking. *Mon. Wea. Rev.*, **110**, 1146–1165.

Horel, J. D., 1984: Complex principal component analysis: Theory and examples. *J. Climate Appl. Meteor.*, **23**, 1660–1673.

Hoskins, B. J., 1983: Modelling of the transient eddies and their feedback on the mean flow. *Large-Scale Dynamical Processes in the Atmosphere.* B. Hoskins and R. Pearce, Eds., Academic Press.

——, I. A. James and G. H. White, 1983: The shape, propagation and mean-flow interaction of large-scale weather systems. *J. Atmos. Sci.*, **40**, 1595–1614.

Kruse, H. A., and K. Hasselmann, 1986: Investigation of processes governing the large-scale variability of the atmosphere using low-order barotropic spectral models as a statistical tool. *Tellus*, **38A**, 12–24.

Metz, W., 1986: Transient cyclone-scale vorticity forcing of blocking highs. *J. Atmos. Sci.*, **43**, 1467–1483.

Preisendorfer, R. W., F. W. Zwiers and T. P. Barnett, 1981: Foundations of prinicpal component selection rules. Ref. Ser. 84-4, Scripps Institution of Oceanography, University of California, 192 pp.

Wallace, J. M., and M. L. Blackmon, 1983: Observations of low-frequency atmospheric variability. *Large-Scale Dynamical Processes in the Atmosphere.* B. Hoskins and R. Pearce, Eds., Academic Press.

Young, R. E., and G. L. Villere, 1985: Nonlinear forcing of planetary scale waves by amplifying unstable baroclinic eddies generated in the troposphere. *J. Atmos. Sci.*, **42**, 1991–2006.